A comparative study of epitaxial InGaAsBi/InP structures using Rutherford Backscattering Spectrometry, X-ray diffraction and Photoluminescence techniques

M. K. Sharpe[1], I. P. Marko[2], D. A. Duffy[2], J. England[1], E. Schneider[1,2], M. Kesaria[3,4], V. Fedorov[3,5], E. Clarke[3], C. H. Tan[3] and S. J. Sweeney[2*]

[1]*Advanced Technology Institute, Ion Beam Centre, University of Surrey, Guildford, GU2 7XH, UK*

[2]*Advanced Technology Institute and Department of Physics, University of Surrey, Guildford, GU2 7XH, UK*

[3]*Department of Electronic and Electrical Engineering, University of Sheffield, Sheffield, S1 4DE, UK*

[4]*Department of Physics and Astronomy, Cardiff University, Cardiff, CF24 3AA, UK (present address)*

[5]*Saint Petersburg Academic University, 194021 St. Petersburg, Russia*

Abstract – In this work we used a combination of photoluminescence (PL), high resolution X-ray diffraction (XRD) and Rutherford backscattering spectrometry (RBS) techniques to investigate material quality and structural properties of MBE-grown InGaAsBi samples (with and without an InGaAs cap layer) with targeted bismuth composition in the 3-4% range. XRD data showed that the InGaAsBi layers are more homogenous in the uncapped samples. For the capped samples, the growth of the InGaAs capped layer at higher temperature affects the quality of the InGaAsBi layer and bismuth distribution in the growth direction. Low temperature PL exhibited multiple emission peaks; the peak energies, widths and relative intensities were used for comparative analysis of the data in line with the XRD and RBS results. RBS data at random orientation together with channelled measurements allowed both an estimation of the bismuth composition as well as analysis of the structural properties. The RBS channelling showed evidence of higher strain due to possible anti-site defects in the capped samples grown at a higher temperature. It is also suggested that the growth of

* corresponding author: s.sweeney@surrey.ac.uk

the capped layer at high temperature causes deterioration of the bismuth-layer quality. The RBS analysis demonstrated evidence of a reduction of homogeneity of uncapped InGaAsBi layers with increasing bismuth concentration. The uncapped higher bismuth concentration sample showed less defined channelling dips suggesting poorer crystal quality and clustering of bismuth on the sample surface.

Journal of Applied Physics

AIP Publishing

Introduction

Adding bismuth into conventional III-V semiconductors gives rise to a large band gap reduction. Substituting arsenic atoms in conventional III-V compounds and alloys with small amounts of bismuth creates an energy state in the host valence band (VB) which interacts with the host valence band states. This causes a valence-band anti-crossing (VBAC) interaction [1]. This strongly reduces the bandgap, E_g, by ~80meV/Bi% and ~56meV/Bi% in GaAsBi and InGaAsBi, respectively [2, 3, 4, 5, 6] and hence opens up possibilities to extend the spectral range of GaAs- and InP-based light emitting and detecting devices into the mid-infrared [4, 6]. At the same time, incorporating bismuth strongly increases the spin-orbit splitting energy separation, Δ_{SO}. This is due to both the effects of an enhanced electron spin-orbital (SO) angular momentum interaction within the heavy bismuth atoms and the upward movement of the valence band maximum. For bismuth compositions for which $\Delta_{SO} > E_g$ the deleterious effects of processes such as Auger recombination (involving excitation of a hot hole into the spin-orbit split off band; the so-called CHSH process) and inter-valence band absorption (IVBA) can be suppressed. These processes limit the performance and efficiency of the near- and mid-infrared photonic devices. Figure 1 presents a summary of experimental data of the compositional dependence of E_g and Δ_{SO} in GaAsBi and InGaAsBi with a fixed indium fraction of 53% as a function of bismuth concentration, which are in good agreement with theoretical VBAC calculations presented in the figure [3, 4, 6]. From these data it is shown that the energy cross-over ($\Delta_{SO} > E_g$) occurs at bismuth concentrations around 10% in GaAsBi [3, 4, 7], and at 3-4% bismuth in InGaAsBi alloy system on InP [5, 6]. Such alloys therefore offer a practical route to reduce, or even eliminate, fundamental loss processes such as Auger recombination and IVBA, which is expected to significantly improve the temperature stability of device output power, with the added benefit of growth on well-established GaAs and InP substrates using well-established III-V device fabrication technologies. GaAsBi/GaAs is suitable for the near-IR, particularly 1.55 μm telecom devices, while InGaAsBi could span a wide spectral range from the near- and mid-IR out to >6μm, while still maintaining tolerable strain levels on standard InP substrates. In addition, for detector applications 3.2% Bi incorporation leads to a cut-off wavelength of about 2.1μm at room temperature [8]. The application of mid-infrared devices on InP is particularly promising owing to the fact that (i) a much

smaller fraction of bismuth is required to achieve the preferential band structure compared to indium, (ii) InGaAsBi/InP heterostructures can exploit well-established conventional InP telecoms device processing, and (iii) the fact that InP substrates are much cheaper and more thermally conductive than GaSb as conventionally used for interband mid-infrared devices.

Despite the inspiring potential of III-V-bismide alloys, there are several main challenges related to practical realisation of bismuth containing photonic devices. These are related to growth issues and difficulty in incorporating large bismuth atoms into the III-V crystal lattice. This requires a reduced growth temperature and consequently leads to a deterioration of the material quality. Wang *et al.* presented a comprehensive review discussing the historical development of epitaxial growth methods of different bismide alloys, discussing in detail most of the challenges and progress in material growth [9]. During the past decade, most of the focus has been on developing near-infrared band gap GaAsBi based structures on GaAs substrates. This has resulted in the demonstration of electrically pumped quantum well (QW) lasers with bismuth compositions of up to 6% and maximum room temperature lasing wavelengths of 1142 nm [10, 11, 12]. The threshold current densities of these devices are relatively high compared to bismuth-free material which has been shown to be due to defect-related recombination [11, 13]. The main limiting factors affecting the devices are non-radiative recombination via defects and inhomogeneity effects caused by low temperature growth and difficulties of bismuth incorporation [14]. Therefore, understanding and optimisation of growth methods for production of high optical quality semiconductor structures remains one of the main tasks for practical deployment of III-V-bismide alloys in device applications.

In this paper, we use photoluminescence (PL) and Rutherford Back Scattering (RBS) techniques in combination with high resolution X-ray diffraction (XRD) for structural characterisation of InGaAsBi/InP based epitaxial structures to understand the effects of growth conditions on bismuth incorporation, crystallographic structure and the optical properties of InGaAsBi/InP based alloys for mid-infrared applications.

InGaAsBi samples and preliminary characterisation using XRD and photoluminescence

A series of four samples were grown using molecular beam epitaxy (MBE) on 2" sulphur-doped n-InP wafers using a VG V80 MBE system. Following oxide removal, a 200 nm undoped and nominally lattice-matched $In_{0.53}Ga_{0.47}As$ buffer layer was grown with a growth rate of 0.63 ML/s at a substrate temperature of 500°C and an As_2 beam equivalent pressure (BEP) of $8x10^{-6}$ mbar (As_2:III ratio of 21:1), with an indium flux of $2.1x10^{-7}$ mbar and a gallium flux of $1.7x10^{-7}$ mbar. The temperature was then lowered for deposition of a 100 nm InGaAsBi layer, at the temperatures specified in table 1. Prior to the growth of the InGaAsBi layer the surface was exposed to a bismuth flux for 30s to soak the surface with bismuth, which was intended to increase bismuth incorporation as previously demonstrated for GaAsBi growth [15, 16]. The InGaAsBi layer was grown using the same indium and gallium fluxes as used for the buffer layer, with a reduced As_2 BEP of $(3.0\pm0.1) \times 10^{-6}$ mbar (As_2:III ratio of 7.9:1) for all samples to allow bismuth incorporation into the layer while avoiding arsenic deficiency during growth (which would lead to a poor surface morphology). The bismuth BEP was intentionally varied between $3.7x10^{-8}$ mbar and $1.2x10^{-7}$ mbar with all other element fluxes kept constant for these samples, resulting in layers of different bismuth compositions. For the samples C1 and C2, the InGaAsBi layer was capped by a 100 nm InGaAs layer grown under nominally the same conditions as the buffer layer, except that the first 20 nm was grown immediately following the InGaAsBi layer at the same substrate temperature, then the temperature was increased to 500°C for the subsequent growth of the remaining 80nm InGaAs. For samples UC1 and UC2, growth was terminated at the end of the InGaAsBi layer.

Table 1: MBE-grown InGaAsBi/InP deposition temperatures and bismuth fluxes for each sample investigated in this work.

Sample Name	Capped or Uncapped	200nm InGaAs Buffer T_{Growth}, °C	100nm InGaAsBi T_{Growth}, °C	InGaAsBi Bismuth flux, mbar	100nm InGaAs Cap T_{Growth}, °C
C1	InGaAs Cap layer	500	370	$1.21x10^{-7}$	20nm at 370, then 80nm at 500
C2	InGaAs Cap layer	500	310	$1.13x10^{-7}$	20nm at 310, then 80nm at 500
UC1	Uncapped	500	310	$3.72x10^{-8}$	
UC2	Uncapped	500	310	$5.5x10^{-8}$	

After growth, the samples were characterised using high resolution X-ray diffraction (XRD), with ω-2θ measurements of the (004) reflection obtained using a Bruker D8 Discover X-ray diffractometer. Fig. 2 shows the XRD patterns for both capped C1 and C2 samples and uncapped UC1 and UC2 samples, along with simulated fits (calculated using the commercial software package X'Pert Epitaxy with lattice constants for GaBi and InBi of 6.324 Å and 6.686 Å, respectively [17]) assuming ideal and homogeneous layers with abrupt interfaces. For each sample, the highest intensity peak at 0" corresponds to the InP substrate. To the left of the substrate peak, a lower angle peak corresponding to the InGaAsBi layer can be observed (except in the case of C1), demonstrating some evidence of bismuth incorporation into the InGaAs host lattice. This results in a lower angle diffraction peak compared to lattice-matched InGaAs due to the increase in lattice constant with substitutional bismuth incorporation. The more distinct Pendellösung fringes around the quaternary layer in the uncapped samples qualitatively suggests a more uniform layer with sharper interfaces than the capped samples, with the degradation in peak intensity and Pendellösung fringe extrema compared to ideal simulations indicating a reduced crystalline quality and/or the presence of interface roughness, respectively.

The capped sample C1 showed no clear peak indicating evidence of bismuth incorporation when modelled using a single uniform layer despite the presence of bismuth flux during the growth, which was attributed to the higher temperature of 370°C compared to 310°C used for the other samples. For the other capped sample (C2), a broad InGaAsBi peak with attenuated Pendellösung fringes potentially indicates some level of relaxation and/or inhomogeneity (an uneven distribution of bismuth) in the InGaAsBi layer [2]. This could be caused by an uneven distribution of bismuth in the InGaAsBi layer, as shown previously for GaAsBi by Reyes et al [18].

In addition to the InGaAsBi peak, in the case of C1, C2, and UC1 a higher angle peak is observed to the right of the substrate. This is attributed to a slight lattice mismatch in the InGaAs cap and/or buffer layer(s) under tensile strain, indicating insufficient indium incorporation during growth.

In the quaternary InGaAsBi alloy both indium and bismuth atoms cause an increase in the lattice constant, hence the exact composition of bismuth cannot be determined unambiguously from a single conventional (004) XRD measurement alone. In Fig. 2, approximate bismuth compositions were

obtained from fitting dynamical diffraction models to the experimental diffraction patterns while assuming fully pseudomorphically strained layers with a fixed indium fraction of 53%. The XRD simulations appear to reproduce the general features of the uncapped samples. However, in the case of the capped samples with less defined broad bismuth features poorer fits were obtained for an ideal multilayer model, which we attribute to the previously speculated inhomogeneity and possible relaxation in the quaternary layer. As additional techniques to characterise the composition of InGaAsBi layers and their quality, we used photoluminescence and RBS measurements. The results of different techniques and their consistency with each other will be presented and discussed further in this paper.

For optical characterisation of the samples we used a photoluminescence setup including a ThermoFisher iS50 FTIR spectrometer, a liquid nitrogen cooled InSb detector, a continuous wave (CW) 532 nm DPSS Laser Quantum Opus laser and a closed cycle He-refrigerator cryostat controlling sample temperature in the range of 10-300 K.

None of the samples showed PL signal at room temperature in the set-up used. Figure 3 presents the PL spectra of all four samples at 15 K under excitation laser power of 950 mW, with spot size of 1.85mm. The PL spectra consisted of multiple peaks, as summarised in Table 2. There are various potential reasons for the multitude of peaks caused by compositional inhomogeneity in both in-plane and growth directions of the InGaAsBi layer, possible presence of localised states and defect related traps discussed below. The spectra were corrected using the system response function but were affected by noise due to strong water absorption in the air over the spectral ranges of 1800-1950nm (0.635-0.689eV) and 2530-2800nm (0.443-0.490eV). To estimate the bismuth composition corresponding to each PL peak, we used the peak shift, ΔE_g, relative to the bandgap of $In_{0.53}Ga_{0.47}As$. This was calculated by subtracting the photon energy of the PL peak from the photon energy peak corresponding to the InGaAs cap or buffer layer. Using the value of ΔE_g and the E_g curve for InGaAsBi in Fig. 1, the corresponding bismuth composition was estimated for each PL peak. Uncertainty of 10-15 meV in the PL peak position would cause an error of 0.2% bismuth as estimated from Fig. 1. The cap/buffer layer PL was the strongest in C1 sample and as much as 50 or more times weaker in the other samples. The maximum temperature, above which the PL signal became

undetectable, are also given in Table 2 for comparison of the samples. Capped sample C1 demonstrated the strongest, but broadest, PL signal with the presence of longer wavelength peaks compared with the bandgap of $In_{0.53}Ga_{0.47}As$ as shown in Table 2, which may indicate incorporation of bismuth as shown in the table. However, given that there was little evidence of bismuth incorporation from XRD, the origin of the long wavelength emission is uncertain in this sample. It may be caused by various reasons including possible localised states with strong PL signal at longer wavelengths at low temperature [5] and/or recombination via defect related traps [19] caused by the low growth temperature. We make a note of caution here that such long-wavelength emission bands may also relate to the low-temperature grown InGaAs layer of the cap as we recently observed in InGaAs p-i-n structures grown at 350^{o}C demonstrating a weak PL emission in the range of 0.4-0.7 eV, which is a focus of further investigations. The formation of bismuth nanocrystals was previously observed in GaAsBi/AlAs superlattices, giving rise to strong PL signals with wavelengths ranging from 1.3 to 1.7 μm after post-growth annealing [20]. It should be noted that the PL signal was independent of position on the wafer in C1, UC1, UC2 samples with small relative variation of intensities of different peaks in C2 sample. For sample C2, the dashed curve in Fig. 3 shows the PL measured away from the wafer centre, whereas the solid lines were obtained from the central part of the wafers, showing evidence of some spatial non-uniformity; this was not observed in the other samples. The resulting values for bismuth compositions estimated from the PL peaks will be discussed later in this paper in comparison with the results of XRD and RBS analysis.

Table 2: PL peak positions obtained from the spectra presented in Fig. 1. The peak shifts, ΔE_g, were calculated by subtracting the photon energies of the PL peak corresponding to the $In_{0.53}Ga_{0.47}As$ cap or buffer layer from the photon energies of each peak. Using value of ΔE_g and E_g curve for InGaAsBi in Fig. 1, a possible bismuth composition was estimated assuming the nominal indium fraction.

Sample	Maximum T, K	PL peak/ emission band, eV	ΔE_g, meV	Bi %
C1	160	0.819 0.689 0.638 0.47-0.63	0 130 181 189-349	0 2.2 3.07 3.22-6.1
C2*	80	0.782 0.713 0.623	37 106 196	0.66 1.8 3.4
UC1	30	0.805 0.784 0.47-0.55	0 21 255-335	0 0.38 4.4-5.86
UC2	15	0.805 0.781 0.462	0 24 343	0 0.4 6.0

*NB: InGaAs buffer/cap layers peak in sample C2 was very weak and poorly defined being close to the position of the well-defined corresponding InGaAs peak in sample C1 (0.819eV), which was used to estimate the ΔE_g values in sample C2.

Rutherford Back Scattering Measurements

XRD and PL characterisation techniques are unable to give a complete picture regarding composition of elements in the InGaAsBi quaternary alloy because both indium and bismuth give rise to a reduced band gap as well as causing an increase in lattice constant, or strain if unrelaxed [6]. To extend the material characterisation we used Rutherford Backscattering Spectrometry (RBS) to more accurately analyse the bismuth content of the InGaAsBi layers and, using channelling measurements, to investigate the crystallographic quality and nature of the defects. The RBS experimental setup used in this work is described in detail elsewhere [21]. Briefly, the technique involved directing a collimated beam of helium ions onto the samples and measuring the number and energy of ions scattered into particular directions using particle detectors. The results reported in this paper measured ions scattered through an angle of 148.6° [22] in an "IBM geometry", where the incident beam, detector position and surface normal were in the same plane. Mounting the sample on a goniometer [21] allowed channelling RBS measurements to be carried out. For random RBS measurements, the goniometer was first aligned so that the beam was directed along the <001> direction of the sample and then rotated by 2° around both the horizontal and vertical axes.

The major energy loss of the primary ions arises from the kinematic factors of their collisions with the sample atoms. The number and energy of scattered ions increases with the mass of the scattering atom. The ions lose further energy through electronic stopping along their inward (pre-collision) paths and then along their outward (post-collision) paths. The final energy of an ion characterises the mass and depth of the scattering atom from which it was scattered.

Bismuth has a significantly larger atomic mass compared to indium, gallium and arsenic, and so ions scattered from bismuth atoms had the highest energies. The helium ion beam energy, chosen to be 4 MeV, allowed the bismuth peak to occur over energies in the RBS spectrum at higher channels than for any signals from other more abundant elements in the sample. This allowed the relatively small number of counts in the peak to be unambiguously assigned to bismuth, without the need to remove significant contributions from other elements. This was possible in both the uncapped (with bismuth in the surface layer) and capped samples (with bismuth in a buried layer). The sensitivity for bismuth was also good because its large mass gave a large RBS cross section and hence relatively high number of scattering events per atom. Previous RBS studies on InGaAsBi by Feng *et al* [23] had used lower ion energies (around 2 MeV) so that the bismuth peak overlapped with the other elements making it harder to unambiguously identify. To demonstrate this effect, Fig. 4 (a) and (b) show the randomly oriented RBS spectra for different ion beam energies of 2 MeV and 4 MeV, respectively, simulated for the $In_{0.53}Ga_{0.47}As/In_yGa_{1-y}As_{1-x}Bi_x/In_{0.53}Ga_{0.47}As/InP$ structure as well as the RBS experimental spectra measured in this work (see Fig. 4(b)). It should be noted that the gallium and arsenic atomic masses are similar and hence their RBS peaks overlap. Whilst the signal from indium near the surface is at higher energies than the gallium and arsenic peaks, the presence of indium in all layers, including the substrate, means that the signal from this element dominates the spectrum.

The bismuth peak is clearly differentiated in the 4MeV beam energy data illustrating the importance of operating at higher beam energies. 4MeV is also a good compromise for bismuth peak separation while still having adequate depth resolution, whereas higher beam energies would further reduce the depth resolution. We also note that this beam energy and intensity did not show any evidence of damage creation in the crystals. The time spent collecting each spectrum was chosen so that the sample was bombarded with 5 μC of helium ions. This charge was a compromise between the

collection of sufficient data for improved counting statistics versus causing damage to the sample. After continuous exposure no difference was observed in the quality of the thin film channelling measurements, indicating minimal damage to the sample epilayers throughout the total set of measurements for this beam energy and charge.

The elemental compositions for each layer of the samples were calculated after simulating the measured random (non-channelled) RBS spectra using the SIMNRA program [24]. With the bismuth feature being fully separated from the other elements, bismuth compositions for the quaternary InGaAsBi layers were obtained with measurement uncertainties of 5% (relative), dominated by counting statistics. Table 3 compares the compositions for indium and bismuth obtained via RBS to the predictions from the XRD and PL data presented earlier in this paper. The RBS data indicates a bismuth fraction of ~1.2% in the capped sample C1, despite the absence of Bi-related feature in the XRD spectrum (see Fig. 2). This sample exhibited very strong broad low temperature PL in spectral range 1750-2800nm, which indicated the presence of localised states. We cannot rule out the possibility of recombination via defect related traps either in InGaAsBi layer itself [19] or the low temperature grown part of the InGaAs cap layer, but usually such emission would have relatively weak intensity due to the longer lifetime of trapped carriers. The other capped sample, C2, grown at a lower temperature, showed weaker PL compared to C1 with significantly reduced long-wavelength emission beyond 1900 nm and demonstrated a better agreement in bismuth composition obtained from PL (1.8% and 3.4% Bi for the main peak at 0.713 eV and weaker broad emission around 0.623 eV, respectively), XRD (3.5% Bi) and RBS (3.2% Bi). The PL signals in the uncapped samples were very weak and detectable only at low temperatures below 30 K, which indicates relatively poor material quality and, consequently, very low PL efficiency. The bismuth compositions implied by the variation of InGaAsBi bandgaps with bismuth compositions (assuming indium composition of 53%) are different from the ones obtained from XRD and RBS and suggests that the origin of the PL may relate to localised states.

Table 3: Elemental percentages obtained from the random RBS for the $In_xGa_{1-x}As_{1-y}Bi_y$ samples. XRD and PL predicted percentages included. The bismuth fractions deduced from the PL results correspond to the PL peaks as given in Table 2.

	XRD		PL		RBS	
Sample	In (%)	Bi (%)	In (%)	Bi (%)	In (%)	Bi (%)
C1	53	0.4% (ambiguous)	53	0 2.2 3.07 3.22-6.1	52	1.2
C2	53	3.5	53	0.66 1.8 3.4	53	3.2
UC1	53	3.1	53	0 0.38 5.5-5.86	53	2.1
UC2	53	4.5	53	0 0.4 6.0	53	3.2

The variation in results may be due to inhomogeneity in bismuth concentration in the layers and the presence of non-substitutional bismuth. Among the reasons causing the relatively higher intensity of the PL spectra from the capped samples C1 and C2 could be the improved quality of the InGaAsBi layer due to annealing effects during the higher temperature cap deposition (that, however, may not always be the case if the growth conditions for capped and uncapped samples are different) and/or improved carrier confinement in the InGaAsBi layer due to the wider band gap InGaAs cap layer. Figure 5 shows the bismuth peaks of the random RBS spectra for all the samples so that the bismuth distributions in the InGaAsBi layers can be compared.

The use of 4MeV as the primary beam energy separates out the bismuth from the other elements in the RBS spectra, but degrades the depth resolution of the measurements (because electronic stopping reduces as primary energy is increased). It is not therefore highly justified to fit the bismuth peak with multiple layers, but a qualitative description of the bismuth distribution can be made by considering the bismuth peak shapes. The shape of the bismuth peak for C1, which is more peaked to lower energies, clearly suggests that there was a higher concentration of bismuth near the base of the InGaAsBi layer than at its surface, unlike C2, whose shape suggests a more homogeneous distribution; the higher bismide layer deposition temperature (370ºC vs 310ºC) appears to have caused bismuth diffusion. The bismuth distribution in UC1 may be slightly more surface peaked than UC2.

The bismuth peaks for the capped samples occur at a smaller channel numbers (energies) compared to the uncapped samples because of the extra energy loss of the primary beam in the cap layers. As shown in Fig. 5 the right-hand tail of the bismuth peak is more drawn out in the capped samples compared to the uncapped samples, suggesting an uneven distribution of bismuth within the InGaAsBi layer.

RBS channelling measurements

To obtain further information on substitutionality and defects in the crystal for the InGaAsBi layer the goniometer was adjusted so that the primary ion beam was aligned along channelling directions (crystallographic axes of the crystal). Fig. 6 compares the aligned (<110> direction) and random RBS spectra for the uncapped samples. The lower yields for the indium, arsenic with gallium, and bismuth peaks from the aligned spectrum compared to the random spectra in Fig. 6, imply that the InGaAsBi layer has reasonable overall crystallinity. UC1 shows a higher variation in the RBS spectrum, compared to UC2. With UC2, a more defective bismide layer, causes helium ion beam scattering such that the channelling in the substrate is reduced and hence closer to that of the random angle measurements.

Channelling dips could be measured by rotating the sample on the goniometer around the vertical direction, changing the incident angle of the beam to the sample. In this technique, regions that represented the signal from elements at particular depths in the sample were chosen in the RBS spectra. The intensities of the integrated signal in these regions were plotted as shown in Fig. 7 and 8 as the goniometer angle was varied by +/- 1.5 degrees around the vertical axis relative to axial channelling directions. This means that the intensities in these plots have been normalised to the intensity along a planar channel direction, rather than to the random direction. Such channelling dips were collected with the beam normal to the sample for the <100> direction, with the goniometer at 45° to the normal for the <110> direction. The <111> direction is located after a rotation around the sample surface normal, with the goniometer tilted at 54.7°. Channelling dips were measured in all three directions for the uncapped samples where the regions in the RBS spectra for the surface bismide layer could easily be defined. In the capped sample spectra, assigning the regions for the

bismide layer beneath the cap was more complicated, so channelling dips were only measured in the <100> (sample normal) direction.

The shape of the channelling dips can be instructive about the sample characteristics. Fig. 7(a) and 7(b) show <100> channelling dips for the C2 (310C) and C1 (370C) samples. Fig. 7(a) shows a channelling dip that is symmetric either side of the minimum with a low intensity suggesting that there were few defects, such as interstitial atoms, present in the channels to scatter the beam. In contrast, Fig. 7(b) shows a shallower channel, indicative of crystal defects. It also suggests a possible steering effect whereby the channelling dip is interrupted by a waveform like pattern on one side [25, 26], with all the elements in the InGaAsBi layer showing two minima. The deepest minimum corresponds to that in the indium of the substrate. The second minimum, not present in the substrate, is often associated with strain [25, 26, 27] or defects. However, as no clear strained layer was resolvable in XRD, the second minimum may be associated with stacking fault related defects as has been observed in metallic alloys [28, 29] and predicted for III-nitrides [30, 31]. Strain relaxation occurs by formation of strain relieving defects, which allows for the average lattice constant in the growth direction to be some value between that of its fully strained (pseudomorphic/tetragonal) and fully relaxed (cubic) values. However, the analysis of XRD and RBS data indicates that there may be some other factors at play. For example, anti-sites, where the group III or V sites have an element from the other site, as has also been seen in GaAs(Bi) [32, 33], may increase the observed lattice mismatch. We speculate that it is also possible that in InGaAsBi, bismuth gives rise to inhomogeneities leading to the formation of clusters or other localised structures in the layer similar to that observed in GaAsBi [20, 34, 35, 36].

Fig. 8 shows the channelling dips for both uncapped samples in the <111> direction. The channelling dips in the other directions (not shown) are similar. The sample UC2 with the higher bismuth content has shallower channelling dips for all elements compared to UC1, indicating a poorer crystal quality or increased primary beam divergence during the measurement (caused by an amorphous surface layer). This is supported by the decreased crystalline scattering observed in XRD along with the sample having the lowest intensity PL further indicating poor crystallinity. Additionally, observations of surface roughness from the SEM images (Fig. 9) showed a non-uniform

surface for UC2 with sub-micron islands and clusters or droplets. This could indicate the presence of droplets in the sample, as previously reported for InGaAsBi [37] and observed in GaAsBi [38]. Sample UC1 had a smooth surface with no visible surface inhomogeneity or defects, which supports the greater crystallinity of this sample shown by XRD and RBS.

Conclusions

In conclusion, using a combination of PL, XRD and RBS measurements, we have investigated the properties of MBE-grown InGaAsBi layers with and without an InGaAs cap layer. Since indium and bismuth have the same effect on the lattice constant, multiple techniques are required to fully interpret the compositional and structural properties of the grown layers.

The use of multiple techniques to determine the bismuth content and structural properties of InGaAsBi samples has been shown to be important. XRD data in this work showed that the InGaAsBi layers are more homogenous in the uncapped samples, whereas the growth of the InGaAs capped layer at higher temperature caused deterioration of the quality of the InGaAsBi layer. PL studies indicated poor optical quality of the material with no detectable PL at room temperature. Low temperature PL exhibited multiple emission peaks, whose positions, width and relative intensities can be used for comparative analysis of the data in line with the XRD and RBS results. Interestingly, both RBS and PL suggest some bismuth incorporation (1.2% bismuth from RBS) in the C1 capped sample grown at a higher temperature of 370^{o}C, for which XRD data did not demonstrate any bismuth-related feature. In this sample, the presence of strain and defects in the InGaAsBi layer was evident from the indium, gallium, arsenic and bismuth channelling dips all exhibiting the steering effect consistent with strain and/or defects in the layer. The RBS results are in agreement with the PL observations, where strong and broad long-wavelength emission band in C1 sample was observed due to recombination via localised states and possible electron traps related to various defects. The second capped sampled (C2) grown at a lower temperature of 310^{o}C exhibited much weaker localised states/traps related emission compared to C1, but showed multiple PL emission peaks at shorter wavelengths, which is associated with a variation of bismuth composition in the growth direction and suggests possibility of uneven bismuth distribution in the InGaAsBi layer due to the annealing effect during the higher

temperature cap layer growth. The lower growth temperature in C2 sample compared to C1, was advantageous in achieving a better crystalline quality and bismuth incorporation.

The two uncapped samples, UC1 and UC2, demonstrated very weak bismuth-related PL features compared to the capped samples (Fig. 3). For the uncapped samples, RBS and XRD data indicated a larger amount of bismuth in UC2 compared to UC1. The RBS analysis demonstrated evidence of a reduction of homogeneity of the InGaAsBi layer with increasing bismuth concentration. The uncapped sample (UC2), with more bismuth, showed poorer quality channelling dips with more scattering at the dip minimum due to poorer crystal quality and clustering of bismuth on the sample surface.

Acknowledgements

This work was supported by the Engineering and Physical Sciences Research Council, U.K. (EPSRC; projects EP/H005587/1 and EP/N021037/1), which also provided a studentship for M. K. Sharpe along with a student training project at the UK National Ion Beam Centre providing beam time funded by the EPSRC (NS/A000059/1).

Figure captions

Fig.1 The room temperature bandgap energy (E_g) and spin-orbit splitting energy (Δ_{SO}) for unstrained $GaAs_{1-y}Bi_y/GaAs$ and $In_{0.53}Ga_{0.47}As_{1-y}Bi_y/InP$. The solid and dashed curves represent VBAC theoretical calculations for case of GaAsBi and InGaAsBi, respectively. The data points show the experimental results (full symbols – GaAsBi/GaAs, open symbols – InGaAsBi/InP) of different authors discussed in detail elsewhere [3, 4, 5, 6].

Fig. 2 XRD scans for the InGaAsBi samples including two uncapped samples UC1 and UC2 and two InGaAs cap layer samples C1 and C2, offset for clarity. Approximate bismuth fractions for each sample are included for fixed indium fractions of 53%, with C1 being poorly reproduced from XRD modelling of a single uniform layer.

Fig. 3 PL spectra of InGaAsBi samples studied in this work measured at 15 K and continuous wave 532 nm laser excitation at 950 mW. The dashed line is the PL spectrum measured from the C2 sample from another position on the wafer closer to its growth edge (the other samples did not show significant variation of PL across the wafer). The spectra for C2, UC1, UC2 are scaled with the scaling factor given near the corresponding sample labels. The insert shows weak PL peaks in sample C2 in more detail.

Fig. 4 Comparison of RBS spectra for (a) 2MeV and (b) 4MeV ion beam energies on an InGaAs capped InGaAsBi sample. Contributions from P, Ga, As, In and Bi are based of simulations, with (b) including the experimental RBS spectra. The bismuth peak is more distinct when using 4MeV ion beam energies.

Fig. 5 Comparison of the bismuth peak in the random angle RBS curves for all InGaAsBi samples. Asymmetry in the bismuth peak may suggest an uneven bismuth distribution in the layer.

Fig. 6 Comparison of the channelling RBS spectra for (a) sample UC1 and (b) sample UC2. The aligned direction is for the <110> and the random is for a tilt of 1.5° and -1.5° either side of the same channel along a fixed axis.

Fig. 7 Channelling RBS dips for two capped InGaAsBi samples. (a) shows the <100> scan for the InGaAs capped InGaAsBi/InP sample(C2) and (b) shows the <100> scan for the other InGaAs capped InGaAsBi/InP sample (C1) with defect peaks in the PL spectra.

Fig. 8 Channelling RBS dips for the uncapped InGaAsBi/InP samples. (a) Show the <111> scan for UC1 sample with less Bi and (b) shows the <111> scan for the UC2 sample with more Bi.

Fig. 9 SEM images of the surface of the uncapped InGaAsBi/InP samples UC1 and UC2.

References

[1] K. Alberi, J. Wu, W. Walukiewicz, K. M. Yu, O. D. Dubon, S. P. Watkins, C. X. Wang, X. Liu, Y.-J. Cho, J. Furdyna, "Valence-band anticrossing in mismatched III-V semiconductor alloys", Phys. Rev. B, **75**, 045203 (2007).

[2] J. P. Petropoulos, Y. Zhong, J. M. O. Zide, "Optical and electrical characterization of InGaBiAs for use as a mid-infrared optoelectronic material", Appl. Phys. Lett., **99**, 031110 (2011).

[3] Z. Batool, K. Hild, T.J.C. Hosea, X.F. Lu, T. Tiedje, S. J. Sweeney, "The electronic band structure of GaBiAs/GaAs layers: Influence of strain and band anti-crossing", *J. Appl. Phys.*, vol. 111, no. 11, 113108, 2012.

[4] S. J. Sweeney, S. R. Jin, "Bismide-nitride alloys: Promising for efficient light emitting devices in the near- and mid-infrared", *J. Appl. Phys.*, vol. 113, 043110, 2013.

[5] I. P. Marko, Z. Batool, K. Hild, S. R. Jin, N. Hossain, T. J. C. Hosea, J. P. Petropoulos, Y. Zhong, P. B. Dongmo, J. M. O. Zide, S. J. Sweeney, "Temperature and Bi-concentration dependence of the bandgap and spin-orbit splitting in InGaBiAs/InP semiconductors for mid-infrared applications", *Applied Physics Letters*, v 101, n 22, 221108, November 26, 2012.

[6] S. R. Jin and S. J. Sweeney, "InGaAsBi alloys on InP for efficient near- and mid-infrared light emitting devices", *J. Appl. Phys.*, vol. 114, 213103, 2013.

[7] M. Usman, C. A. Broderick, A. Lindsay, E. P. O'Reilly, "Tight-binding analysis of the electronic structure of dilute bismide alloys of GaP and GaAs", *Phys. Rev. B*, vol. 84, 245202, 2011.

[8] Y. Gu, Y. G. Zhanga, X. Y. Chen, Y. J. Ma, S. P. Xi, B. Du, and Hsby. Li, "Nearly lattice-matched short-wave infrared InGaAsBi detectors on InP", Appl. Phys. Lett. **108**, 032102, 2016.

[9] L. Wang, L. Zhang, L. Yue, D. Liang, X. Chen, Y. Li, P. Lu, J. Shao, S. Wang, "Novel Dilute Bismide, Epitaxy, Physical Properties and Device Application", *Crystals* 2017, vol. 7 (3), 63, 2017.

[10] I. P. Marko, S. R. Jin, K. Hild, Z. Batool, Z. L. Bushell, P. Ludewig, W. Stolz, K. Volz, R. Butkutė, V. Pačebutas, A. Geizutis, A. Krotkus, S. J. Sweeney, "Properties of hybrid MOVPE/MBE grown GaAsBi/GaAs based near-infrared emitting quantum well lasers", *Semicond. Sci. Technol.*, vol. 30, 094008, 2015.

[11] I. P. Marko, S. J. Sweeney, "Progress Toward III–V Bismide Alloys for Near- and Midinfrared Laser Diodes", IEEE Journal of Selected Topics in Quantum Electronics, V. 23, Iss. 6, 1501512 (2017).

[12] X. Wu, W. Pan, Z. Zhang, Y. Li, C. Cao, J. Liu, L. Zhang, Y. Song, H. Ou, S. Wang, "1.142 μm GaAsBi/GaAs Quantum Well Lasers Grown by Molecular Beam Epitaxy", ACS Photonics **4** (6), 1322-1326 (2017).

[13] I. P. Marko, P. Ludewig, Z. L. Bushell, S. R. Jin, K. Hild, Z. Batool, S. Reinhard, L. Nattermann, W. Stolz, K. Volz, S. J. Sweeney "Physical properties and optimization of GaBiAs/(Al)GaAs based near-infrared laser diodes grown by MOVPE with up to 4.4% Bi", *J. Phys. D: Appl. Phys*., **47**, 345103 (2014).

[14] I. P. Marko, S. J. Sweeney, "The influence of inhomogeneities and defects on novel Quantum Well and Quantum Dot based infrared-emitting semiconductor lasers", *Semiconductor Science and Technology*, **33**, 113002(15pp), 2018.

[15] T. B. O. Rockett *et al.*, "Influence of growth conditions on the structural and opto-electronic quality of GaAsBi," *J. Cryst. Growth*, vol. 477, pp. 139–143, 2017.

[16] R. B. Lewis, M. Masnadi-Shirazi, and T. Tiedje, "Growth of high Bi concentration $GaAs_{1-x}Bi_x$ by molecular beam epitaxy," *Appl. Phys. Lett.*, vol. 101, no. 8, pp. 1–5, 2012.

[17] A. Janotti, S. H. Wei, and S. B. Zhang, "Theoretical study of the effects of isovalent coalloying of Bi and N in GaAs," *Phys. Rev. B - Condens. Matter Mater. Phys.*, vol. 65, no. 11, pp. 1–5, 2002.

[18] D F Reyes, F Bastiman, C J Hunter, D L Sales, A M Sanchez, J PR David and D González, "Bismuth incorporation and the role of ordering in GaAsBi/GaAs structures", Nanoscale Research Letters 2014, 9:23.

[19] Ł. Gelczuk, J. Kopaczek, T. B. O. Rockett, R. D. Richards & R. Kudrawiec, "Deep-level defects in n-type GaAsBi alloys grown by molecular beam epitaxy at low temperature and their influence on optical properties", Scientific Reports, **7**, 12824, 2017.

[20] R. Butkutė, G. Niaura, E. Pozingytė, B. Čechavičius, A. Selskis, M. Skapas, V. Karpus, A. Krotkus, "Bismuth Quantum Dots in Annealed GaAsBi/AlAs Quantum Wells", *Nanoscale Research Letters*, 12:436, (2017).

[21] A. Simon, C. Jeynes, R. P. Webb, R. Finnis, Z. Tabatabian, P. J. Sellin, M. B. H. Breese, D. F. Fellows, R. van den Broek and R. M. Gwilliam, The new Surrey ion beam analysis facility, Nucl. Instrum. Methods Phys. Res., Sect. B, 2004, 219, 405–409.

[22] M. Mayer "Rutherford Backscattering Spectrometry (RBS)", Lectures given at the Workshop on Nuclear Data for Science and Technology: Materials Analysis Trieste, 19-30 May 2003

[23] G. Feng, K. Oe and M. Yoshimoto, "Bismuth containing III-V quaternary alloy InGaAsBi grown by MBE, *Phys. Stat. Sol*. (a) 203, 11, 2670-2673, 2006.
[24] M. Mayer, "SIMNRA, a Simulation Program for the Analysis of NRA, RBS and ERDA," *American Institute of Physics Conference Proceedings,* vol. 475, p. 541, 1999.
[25] S. Hashimoto, et al. "Steering effect at a strained $NiSi_2$/Si (001) Interface", B13, pp.45-50, 1986
[26] A. Vantomme, "50 years of ion channeling in materials science, Nuclear Instruments and Methods in Physics Research, B 371, pp.12–26, 2016
[27] K. Lorenz, et al., "Anomalous Ion Channelling in AlInN/GaN bilayers: Determination of the strain state", Physics Review Letters, 97, 085501, 2006
[28] C. Lu *et al. "*Direct Observation of Defect Range and Evolution in Ion-Irradiated Single Crystalline Ni and Ni Binary Alloys", *Sci. Rep.* **6**, 19994, 2016.
[29] S. Zhang, K. Nordlund, F. Djurabekova, Y. Zhang, G. Velisa, T. S. Wang, "Simulation of Rutherford backscattering spectrometry from arbitrary atom structures", Phys. Rev. E **94**, 043319, 2016.
[30] M. A. Rana, "Ion channelling studies of defect formation in GaN and related materials", PhD thesis, Department of Physics, National University of Singapore, 2005.
[31] A. Turos, L. Nowicki, A. Stonert, "Ion Channeling Study Of Defects In Multicomponent semiconductor Compounds", International Atomic Energy Agency, Vienna (Austria); INIS vol. 33, INIS no. 32, ISSN 1011-4289; Worldcat; Jun 2002; 83-96, 2002.
[32] J. I. Landman, "Antisite-Related Defects in GaAs Grown at Low Temperatures", PRL, vol 74, no 20, 1995
[33] D. Dagnelund, J. Puustinen, M. Guina, W. M. Chen, I. A. Buyanova, "Identification of an isolated arsenic antisite defect in GaAsBi", *Appl. Phys. Lett.* **104**, 052110 (2014);
[34] J. Puustinen, M. Wu, E. Luna, A. Schramm, P. Laukkanen, M. Laitinen, T. Sajavaara, and M. Guina, "Variation of lattice constant and clusterformation in GaAsBi", J. Appl. Phys. 114, 243504 (2013).
[35] M. Wu, "Observation of atomic ordering of tripleperiod A and -B type in GaAsBi", Appl. Phys. Lett. 105, 041602 (2014)
[36] E. Luna, "Spontaneous formation of nanostructures by surface spinodal decomposition in GaAs1−xBix epilayers", J. Appl. Phys. 117, 185302 (2015)
[37] Y. Zhong, P. B. Dongmo, J. P. Petropoulos, J. M. O. Zide, "Effects of molecular beam epitaxy growth conditions on composition and optical properties of InxGa1−xBiyAs1−y", *Appl. Phys. Lett.* **100**, 112110 (2012)
[38] E.Sterzer, N.Knaub, P.Ludewig, R.Straubinger, A.Beyer, K.Volz, "Investigation of the microstructure of metallic droplets on Ga(AsBi)/GaAs", Journal of Crystal Growth, **408**, pp 71-77, 2014,

AIP Publishing

Journal of Applied Physics

ACCEPTED MANUSCRIPT

This is the author's peer reviewed, accepted manuscript. However, the online version of record will be different from this version once it has been copyedited and typeset.
PLEASE CITE THIS ARTICLE AS DOI: 10.1063/1.5109653

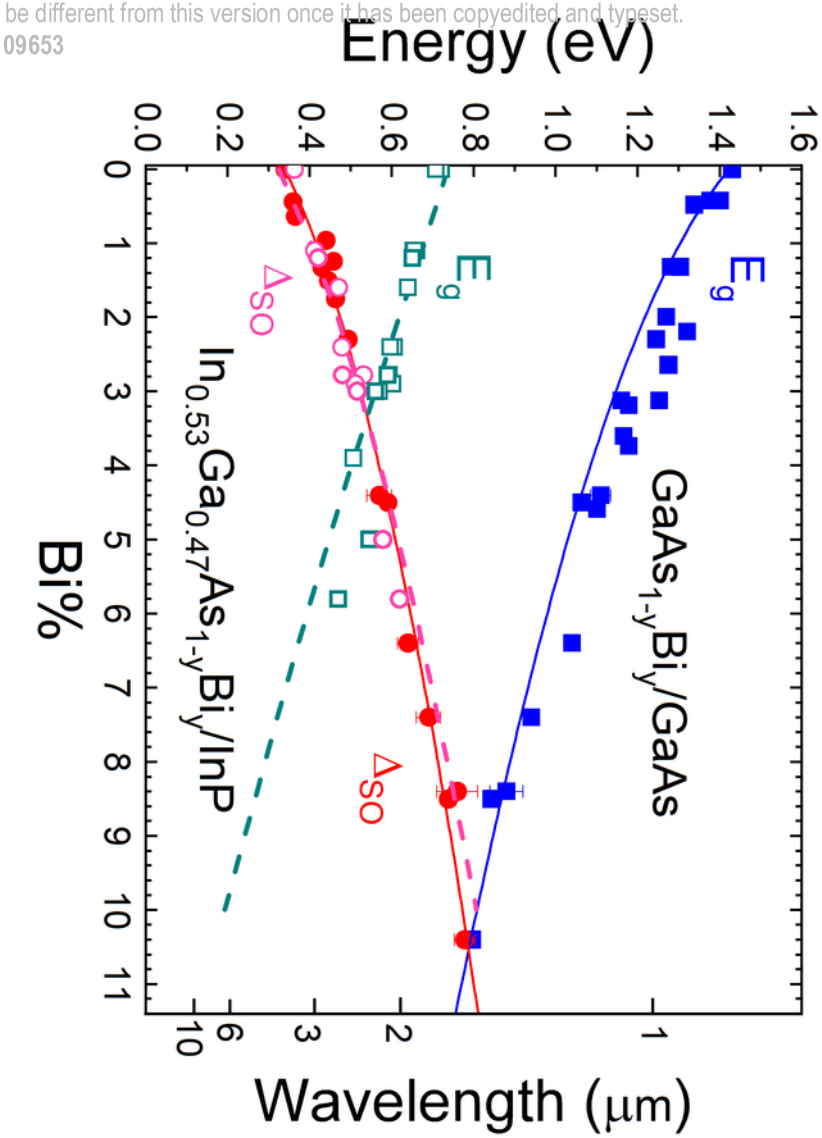

AIP Publishing

Journal of Applied Physics

PLEASE CITE THIS ARTICLE AS DOI: 10.1063/1.5109653

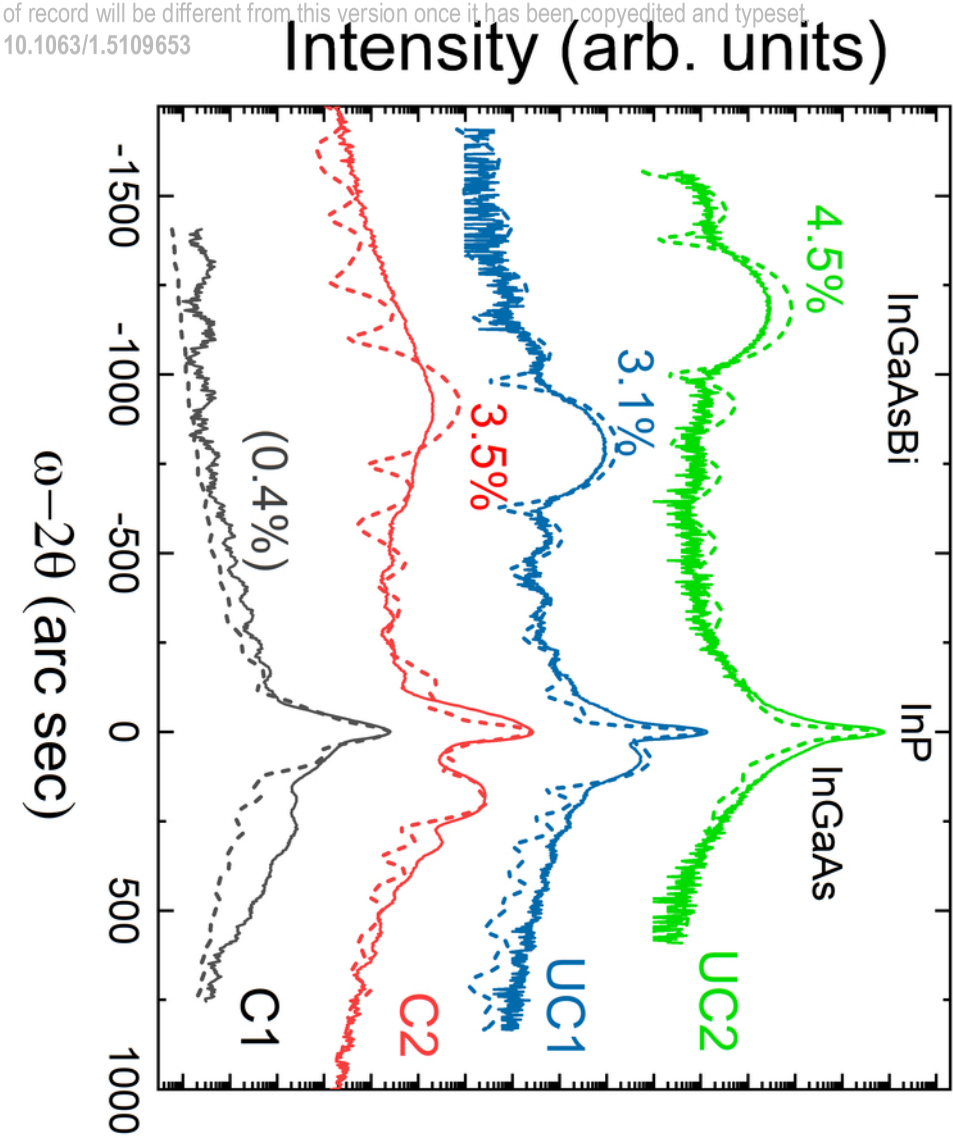

Journal of Applied Physics

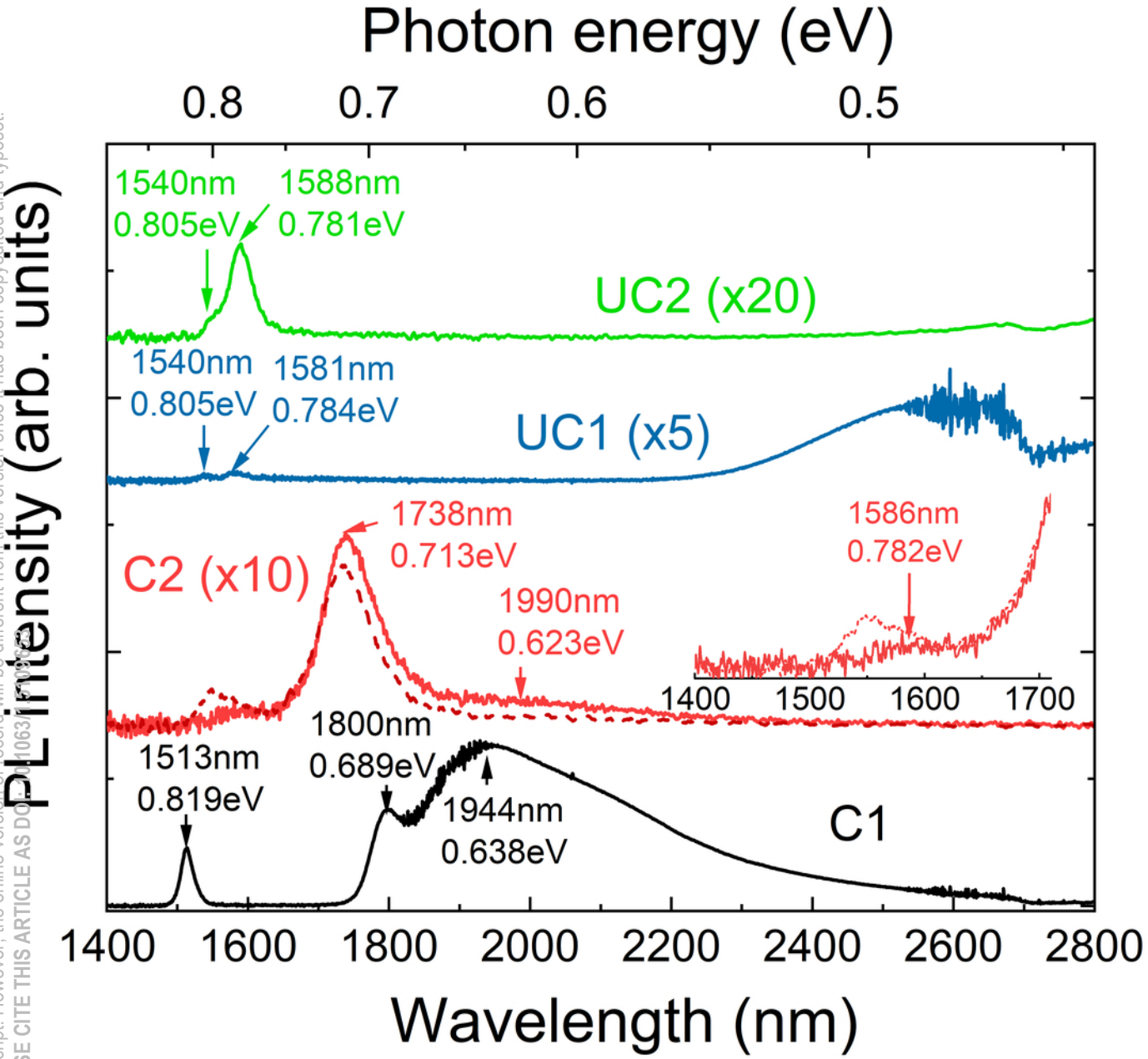

AIP Publishing

Journal of Applied Physics

PLEASE CITE THIS ARTICLE AS DOI: 10.1063/1.5109653

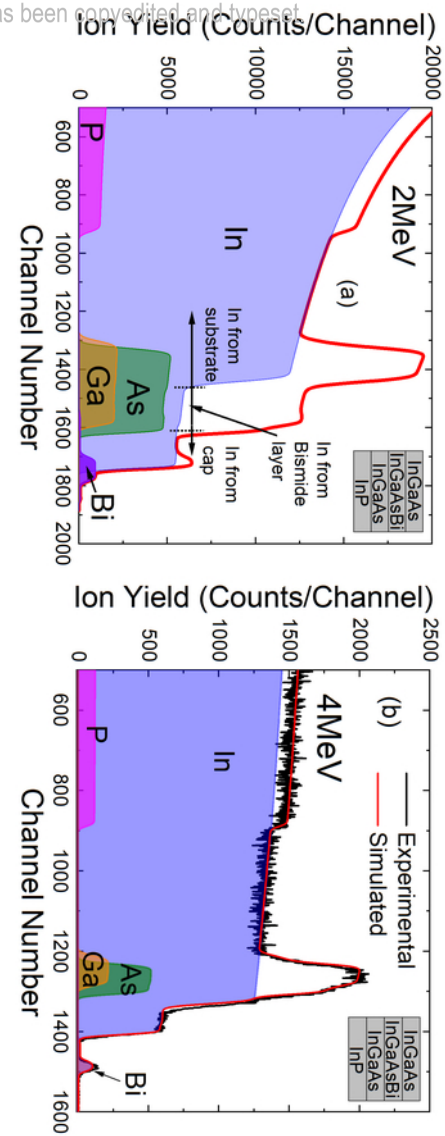

AIP Publishing

Journal of Applied Physics

PLEASE CITE THIS ARTICLE AS DOI: 10.1063/1.5109653

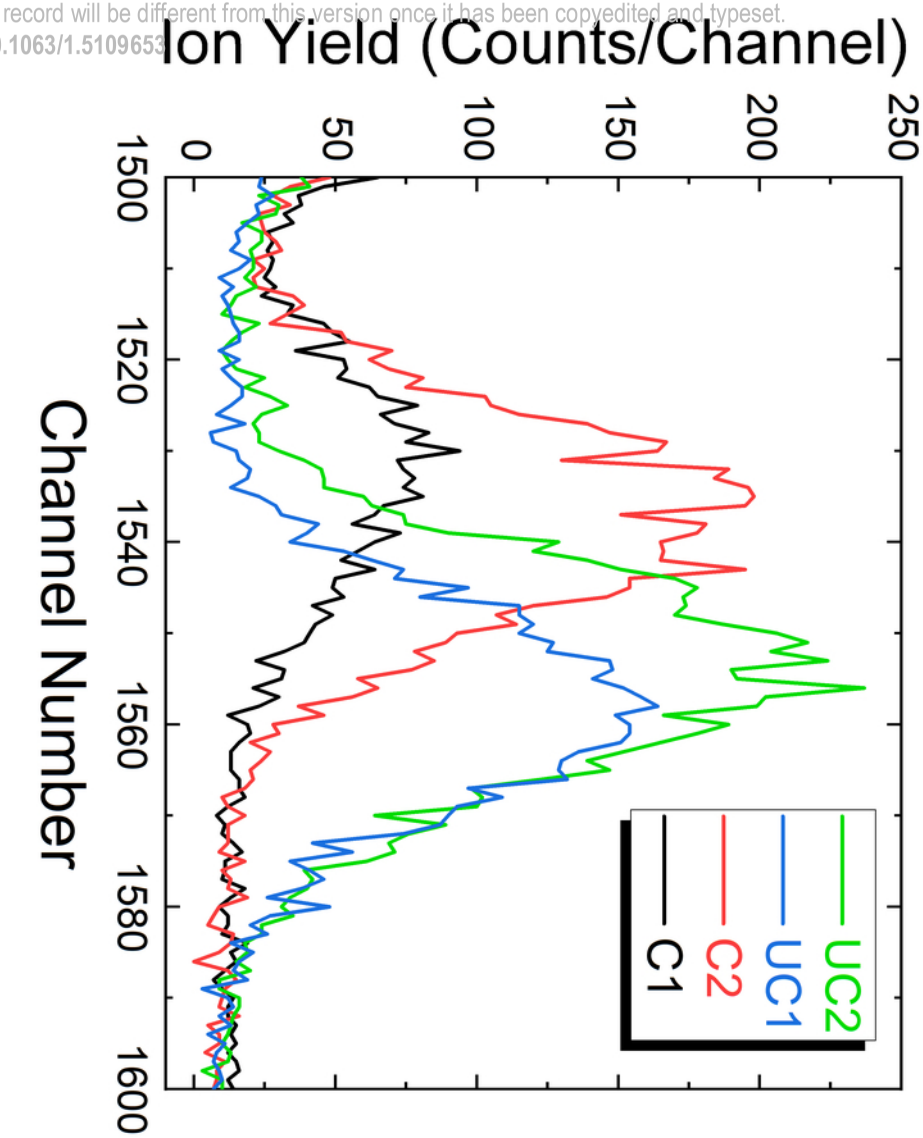

Journal of Applied Physics

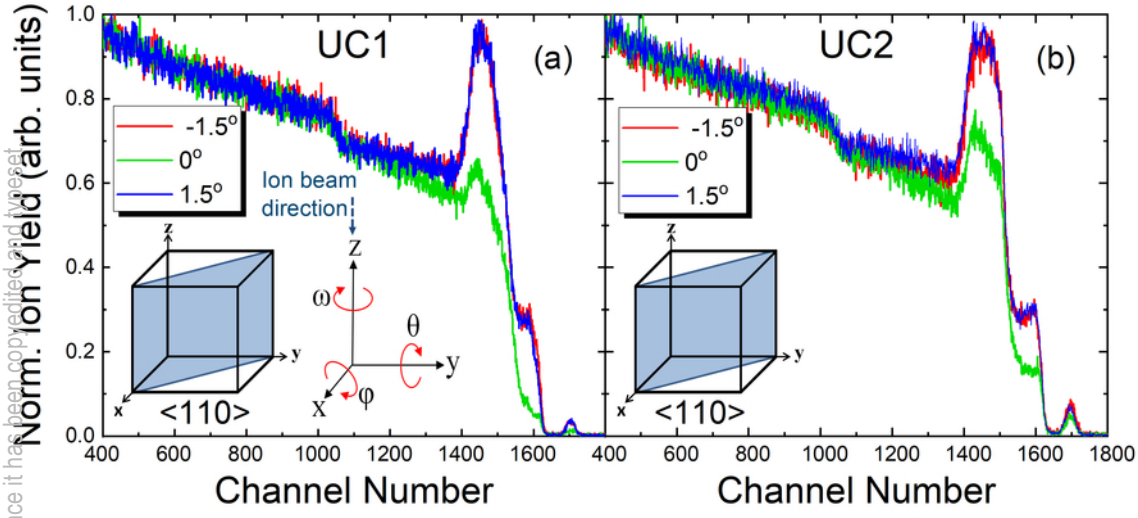

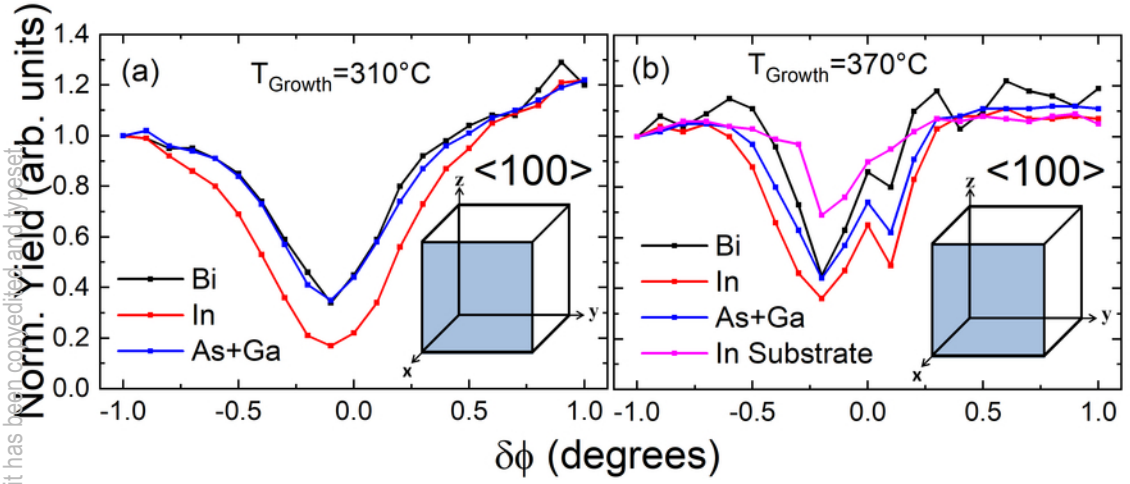

Journal of Applied Physics
AIP Publishing

Journal of Applied Physics

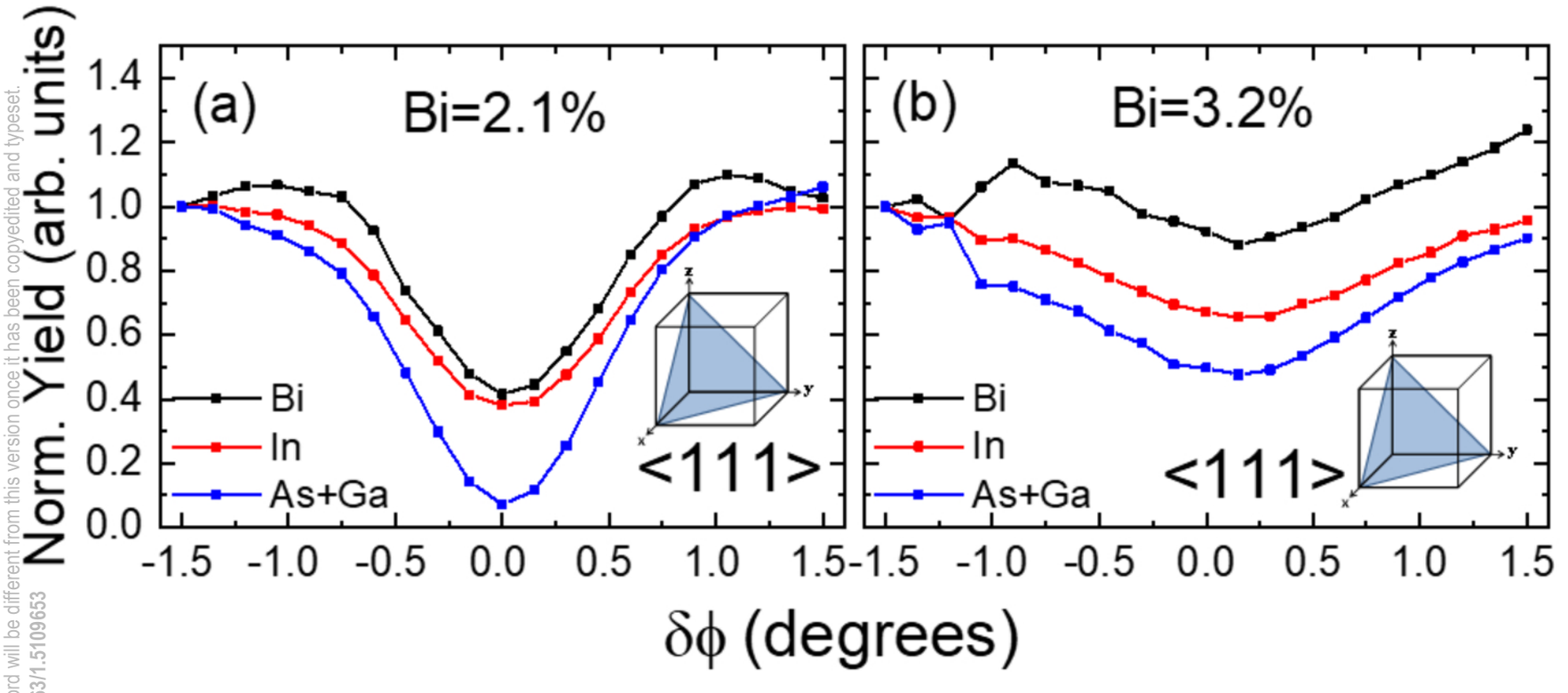

AIP Publishing

Journal of Applied Physics

ACCEPTED MANUSCRIPT

PLEASE CITE THIS ARTICLE AS DOI: 10.1063/1.5129653